# Shape optimization of a cyclone separator using multi-objective surrogate-based optimization

Prashant Singh [a,*], Ivo Couckuyt [a], Khairy Elsayed [b,c], Dirk Deschrijver [a], Tom Dhaene [a]

[a] Department of Information Technology (INTEC), Ghent University-iMinds, Gaston Crommenlaan 8 Blok C0 bus 201, Ghent 9050, Belgium
[b] Department of Mechanical Engineering, Vrije Universiteit Brussel, Research Group Fluid Mechanics and Thermodynamics, Pleinlaan 2, Brussels 1050, Belgium
[c] Mechanical Power Engineering Department, Faculty of Engineering at El-Mattaria, Helwan University, Masaken El-Helmia P.O., Cairo 11718, Egypt

## ARTICLE INFO

## ABSTRACT

Cyclones are one of the most widely used separators in many industrial applications. A low mass loading gas cyclone has two performance parameters, the Euler and Stokes numbers. These indices are highly sensitive to the geometrical design parameters which makes designing cyclones a challenging problem. This paper couples three surrogate models (Kriging, radial basis functions and support vector regression) with the efficient multi-objective optimization (EMO) algorithm to identify a Pareto front of cyclone designs with a minimal number of simulations. The EMO algorithm has been extended to select multiple samples per iteration (as opposed to one in the original formulation) and the ability to use an ensemble of surrogate models. The impact of using different surrogate model types is tested using well-known mathematical models of cyclone separators. The algorithm is applied to optimize the cyclone geometry, parametrized by seven design variables, and compared against the well-known NSGA-II algorithm. The results indicate that the Pareto set designs found using EMO outperform the designs found using NSGA-II while using significantly fewer function evaluations. This translates into substantial savings in time when computationally expensive CFD simulations are used.

## 1. Introduction

Gas cyclones are widely used in air pollution control, gas-solid separation for aerosol sampling and industrial applications. With the advantages of being relatively simple to fabricate, having a low cost to operate, and being adaptable to extremely harsh conditions of high pressure and temperature, cyclone separators have become one of the most important particle removal devices used in scientific and engineering applications. Cyclones are frequently used as final collectors where large particles are to be caught. Efficiency is generally good for dust where particles are larger than about 5 μm in diameter. They can also be used as pre-cleaners for a more efficient collector such as an electrostatic precipitator, scrubber or fabric filter [1].

In cyclone separators, a strong swirling turbulent flow is used to separate phases with different densities. The efficiency of a separator depends upon the cyclone geometry. Optimizing cyclone geometry can be a time consuming exercise. Using

---

* Corresponding author. Tel.: +32 9 33 14986; fax: +32 9 264 3593.
  *E-mail address:* prashant.singh@intec.ugent.be (P. Singh).

**Nomenclature**

| | |
|---|---|
| $a$ | cyclone inlet height [m] |
| $b$ | cyclone inlet width [m] |
| $B_c$ | cyclone cone-tip diameter [m] |
| $d$ | number of design variables [–] |
| $D$ | barrel diameter [m] |
| $D_x$ | vortex finder diameter [m] |
| $e_k$ | SVM slack variables |
| $\mathcal{H}$ | hypervolume indicator |
| $h$ | cylindrical part height [m] |
| $H_t$ | cyclone total height [m] |
| $n$ | number of sample points [–] |
| $\mathcal{P}$ | Pareto set |
| $Q_{in}$ | gas volume flow rate [m³/s] |
| $s$ | standard deviation of model prediction |
| $S$ | vortex finder length [m] |
| $V_{in}$ | area-average inlet velocity [m/s] |
| **x** | data instance |
| $\hat{y}$ | mean of model prediction |
| $Y$ | random variable |

*Greek letters*

| | |
|---|---|
| $\gamma$ | SVM cost parameter |
| $\Delta P$ | pressure drop [N/m²] |
| $\epsilon$ | distance threshold |
| $\mu$ | dynamic viscosity [kg/(m s)] |
| $\phi(\cdot)$ | transformation function |
| $\Phi \cdot$ | normal cumulative distribution function |
| $\psi^{(i)}$ | correlations between $Y(\mathbf{x})$ at the point to be predicted and at the sample data points |
| $\rho$ | gas density [kg/m³] |
| $\sigma^2$ | variance |
| $\theta$ | Kriging hyper-parameter variables |

*Dimensionless numbers*

| | |
|---|---|
| $E_u$ | Euler number |
| $Re$ | Reynolds number |

*Abbreviations*

| | |
|---|---|
| CFD | computational fluid dynamics |
| EMO | efficient multi-objective optimization |
| GA | genetic algorithm |
| KG | Kriging |
| LDA | laser Doppler anemometry |
| LHS | Latin hypercube sampling |
| LS-SVM | least squares support vector machines |
| MLE | maximum likelihood estimation |
| MM | Muschelknautz method of modeling |
| MOEA | multi-objective evolutionary algorithm |
| NSGA-II | non-dominated sorting genetic algorithm 2 |
| PIV | particle image velocimetry |
| PoI | probability of improvement |
| RBF | radial basis function |
| SVM | support vector machines |
| SVR | support vector regression |
| SBO | surrogate based optimization |

Multi-Objective Evolutionary Algorithms (MOEAs) is not desirable since they typically require a large number of objective function evaluations during the optimization process.

Surrogate modeling, also known as metamodeling, is a proven approach to speed up complex optimization problems [2,3]. Surrogate models, or metamodels, are mathematical approximation models that mimic the behavior of (possibly computationally expensive) simulation codes such as mechanical or electrical finite element simulations, analytical models, or computational fluid dynamics (CFD).

While several types of surrogate modeling use-cases can be identified, this work is concerned with the integration of surrogate models into the optimization process, often denoted by surrogate based optimization (SBO). SBO methods typically generate surrogate models on the fly that are only accurate in certain regions of the input space, e.g., around potentially optimal regions. The intermediate surrogate models can then be used to intelligently guide the optimization process to the global optimum. This paper deals with the use of surrogate models for expediting the multi-objective optimization of deterministic black-box problems.

Popular surrogate model types include Kriging [4], radial basis function (RBF) models [5], support vector regression (SVR) models [6], artificial neural networks (ANN) [7], Splines, etc. This work introduces the use of SVR and RBF models in the efficient multi-objective optimization (EMO) algorithm [8]. Kriging, RBF and SVR models are compared with regard to the Pareto set obtained using the EMO algorithm. Also, a new method is proposed that builds multiple heterogeneous surrogate models and uses the most accurate one in each iteration of the EMO algorithm [9].

CFD simulations are often computationally very expensive and optimization of cyclone geometry can take several months. For the intended purpose of analysis and performance evaluation, mathematical models of cyclone separators are used in this work that are substantially cheaper to evaluate. The intent of the work is to validate the performance of the EMO algorithm for optimization of cyclone geometry, and study how Kriging, RBF and SVR models affect the performance. A practitioner can then make an informed decision about the choice of surrogate models when optimization is performed using expensive CFD simulations.

The following section gives a brief introduction to Kriging, RBF and SVR models. Section 3 explains the EMO algorithm. Section 4 introduces the shape optimization problem for a cyclone separator. Section 5 describes the experimental settings while Section 6 discusses the results of the proposed multi-objective optimization scheme. Section 7 concludes the paper.

## 2. Surrogate models

Surrogate-based optimization (SBO) methods have proven themselves to be effective in solving complex optimization problems, and are increasingly being used in different fields [10–13]. Unlike evolutionary multi-objective algorithms such as NSGA-II [14], SMS-EMOA [15] and SPEA2 [16], surrogate-based methods typically require very few function evaluations to converge. This makes surrogate-based methods very attractive for solving optimization problems where the system behavior is expensive to simulate. Surrogate models used in this work include Kriging, RBF and SVR models. A brief introduction to the models is presented below.

### 2.1. Kriging

Kriging models are very popular in engineering design optimization [17]. This is partly due to the fact that Kriging models provide the mean and prediction variance which can be exploited by statistical sampling criteria. Their popularity also stems from the fact that many implementations are widely available [18–21].

Let us assume a set of $n$ samples $X = (\mathbf{x}_1, \ldots, \mathbf{x}_n)'$ in $d$ dimensions having the target values $\mathbf{y} = (y_1, \ldots, y_n)'$. The prediction mean and prediction variance of Kriging are derived, respectively, as,

$$\hat{y}(\mathbf{x}) = \alpha + r(\mathbf{x}) \cdot \Psi^{-1} \cdot (\mathbf{y} - \mathbf{1}\alpha), \tag{1}$$

$$s^2(\mathbf{x}) = \sigma^2 \left( 1 - r(\mathbf{x})\Psi^{-1}r(\mathbf{x})^\top + \frac{(1 - \mathbf{1}^\top \Psi^{-1} r(\mathbf{x})^\top)}{\mathbf{1}^\top \Psi^{-1} \mathbf{1}} \right), \tag{2}$$

where $\mathbf{1}$ is a vector of ones, $\alpha$ is the coefficient of the constant regression function, determined by generalized least squares (GLS), $r(\mathbf{x})$ is a $1 \times n$ vector of correlations between the point $\mathbf{x}$ and the samples $X$, and $\sigma^2 = \frac{1}{n}(\mathbf{y} - \mathbf{1}\alpha)^\top \Psi^{-1}(\mathbf{y} - \mathbf{1}\alpha)$ is the variance.

$\Psi$ is a $n \times n$ correlation matrix of the samples $X$,

$$\Psi = \begin{pmatrix} \psi(\mathbf{x}_1, \mathbf{x}_1) & \ldots & \psi(\mathbf{x}_1, \mathbf{x}_n) \\ \vdots & \ddots & \vdots \\ \psi(\mathbf{x}_n, \mathbf{x}_1) & \ldots & \psi(\mathbf{x}_n, \mathbf{x}_n) \end{pmatrix},$$

with $\psi$ being the correlation function. The correlation function greatly affects the accuracy of the Kriging model used for experiments and in this work the Matérn correlation function [22] with $\nu = \frac{3}{2}$ is used,

$$\psi(\mathbf{x}_a, \mathbf{x}_b)^{Matérn}_{\nu=3/2} = \left(1 + \sqrt{3}l\right) \exp\left(-\sqrt{3}l\right),$$

with $l = \sqrt{\sum_{i=1}^{d} \theta_i(x_a^i - x_b^i)^2}$. The hyperparameters $\theta$ are identified using maximum likelihood estimation (MLE).

## 2.2. Radial basis function models

Radial basis function (RBF) models represent unknown functions as weighted sums of several basis functions. The basis functions are of the form $\phi(\|\mathbf{x} - \mathbf{x}_i\|)$ where $\mathbf{x}$ is a test point, and $\phi(\cdot)$ is a transformation function. The $i^{th}$ basis function depends only on the distance between $\mathbf{x}$ and $\mathbf{x}_i$. Subsequently, the predictor is a linear combination of the basis functions [5],

$$\hat{y} = \hat{f}(\mathbf{x}) = \sum_{i=1}^{n} w_i \phi(\|\mathbf{x} - \mathbf{x}_i\|).$$

The weights $w_i$ have to be found such that,

$$\hat{f}(\mathbf{x}_j) = \sum_{i=1}^{n} w_i \phi(\|\mathbf{x}_j - \mathbf{x}_i\|) = y_j, \quad \forall j = [1, \ldots, n]. \tag{3}$$

Defining a weight vector $\mathbf{w} = [w_1, w_2, \ldots, w_n]^T$ and the matrix $\Phi_{i,j} = \phi(\|\mathbf{x}_j - \mathbf{x}_i\|)$, Eq. 3 can be written as $\Phi\mathbf{w} = \mathbf{y}^T$. The weights can be computed using Eq. 3 as $\mathbf{w} = \Phi^{-1}\mathbf{y}^T$, assuming that $\Phi$ is invertible.

Although different basis functions $\phi(\cdot)$ exist, this work is concerned with Gaussian basis functions of the form [5],

$$\phi(r) = exp\left(\frac{-r^2}{2\sigma^2}\right).$$

For the experiments in this paper, the hyperparameters $\sigma$ and $r$ were found using the DIRECT optimization algorithm [23] and cross-validation. Let $\boldsymbol{\phi} = [\phi(\|\mathbf{x} - \mathbf{x}_i\|], \forall i = 1..n$. The prediction and variance of prediction of a point $\mathbf{x}$ can be obtained as,

$$\hat{y}(\mathbf{x}) = \boldsymbol{\phi}\mathbf{w}, \tag{4}$$

$$s^2(\mathbf{x}) = 1 - \boldsymbol{\phi}\Phi^{-1}\boldsymbol{\phi}^T. \tag{5}$$

For more details about RBF, the interested reader is referred to Sóbester et al. [5].

## 2.3. Least squares support vector machines

Support vector machine (SVM) models are extremely popular due to their generalization abilities and proven empirical performance [24]. SVMs map data into a higher dimensional input space where an optimal separating hyperplane is constructed by solving a quadratic programming problem. Least squares support vector machine [25] (LS-SVM) classifiers are a variant of SVM classifiers which involve solving a system of linear equations instead of the quadratic programming problem as in the original formulation. LS-SVM classifiers have also been extended to solve regression problems, and we use the formulation proposed by Suykens et al. [26].

It is possible to obtain the mean and variance of the prediction from LS-SVM regressors [27] (henceforth referred to as SVR). A detailed discussion on the process of computing mean and variance is out of scope of this work, and the reader is referred to Van Gestel et al. [27].

## 3. Efficient multi-objective optimization (EMO)

The expected improvement and Probability of Improvement (PoI) criteria are widely used for single-objective optimization [28,29]. Recently, multi-objective versions of these criteria are increasingly being used to solve complex multi-objective optimization methods [30,31]. While they have been used in SBO schemes, due to the computational requirements their applicability in practice has been limited to problems with 2 objectives. The recently introduced EMO algorithm [31] provides an efficient computation procedure and can be applied to problems up to about 7 objectives.

A flowchart of the EMO algorithm is shown in Fig. 1. The algorithm begins with the generation of an initial set of points $X$ corresponding to different cyclone geometries. The initial points are evaluated on the expensive objective functions $f_j(\mathbf{x})$, for $j = 1 \ldots m$ corresponding to the performance characteristics of the cyclone separator. Each objective function $f_j(\mathbf{x})$ is then approximated by a surrogate model. Based on the models, useful criteria can be constructed that help in identifying Pareto-optimal solutions. The criteria are used to select a new point in the design space, which is evaluated on the expensive objective functions $f_j(\mathbf{x})$. The models are then updated with this new information and this process is repeated in an iterative manner until some stopping criterion is met.

This work adopts the hypervolume-based PoI criterion. It is important to note that the computation of these criteria requires a prediction of the modeling uncertainty. Hence, the choice of surrogate model is limited to those which can provide the uncertainty of the prediction.
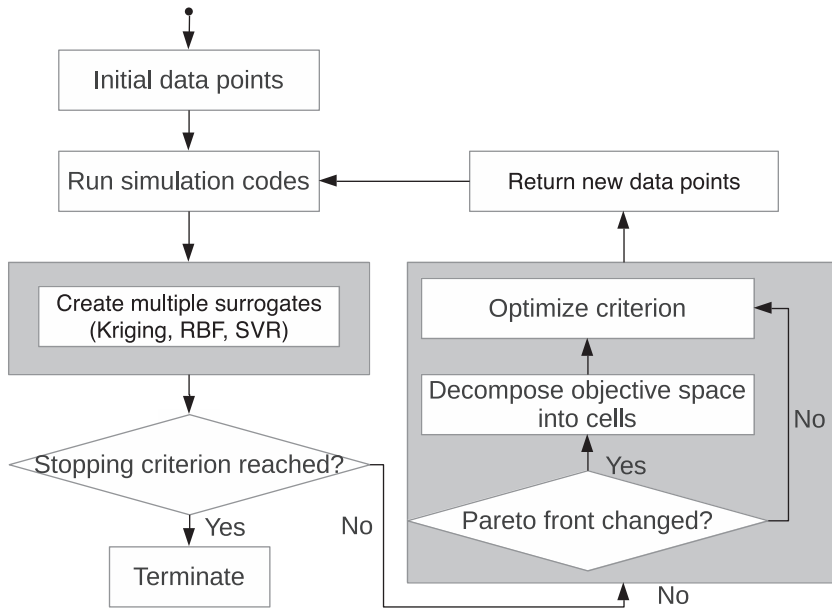
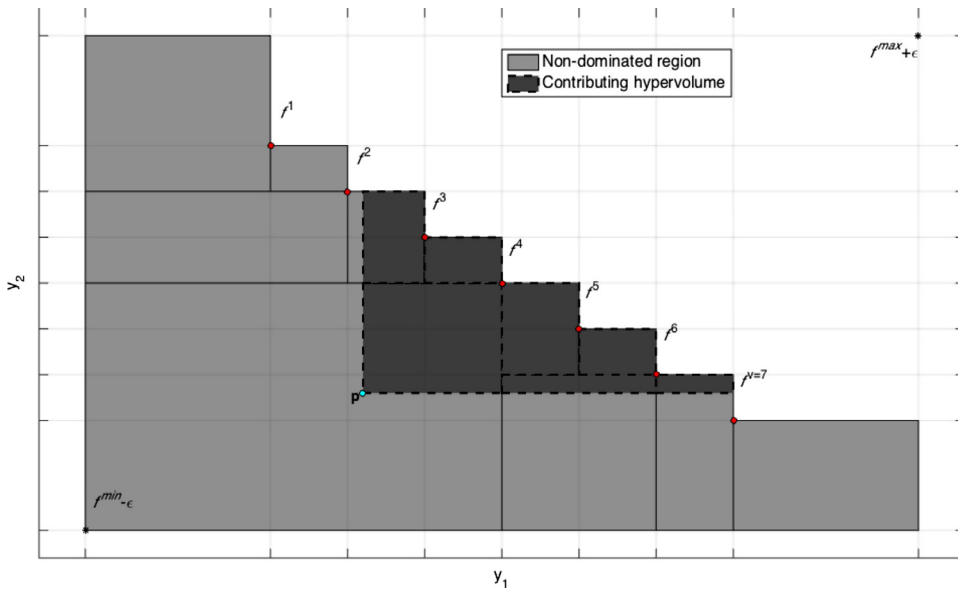**Fig. 1.** Flow chart of the efficient multi-objective optimization (EMO) algorithm.



**Fig. 2.** A Pareto set for two objectives consisting of Pareto points $f^i$, for $i = 1...v$. $f^{min}$ and $f^{max}$ denote the ideal and anti-ideal point respectively. The hypervolume corresponding to the Pareto set is the dark and light shaded region, while the contributing hypervolume is the dark shaded region.

### 3.1. Hypervolume-based probability of improvement

In a multi-objective setting the improvement $I$ over the current Pareto set $\mathcal{P}$ can be defined in several ways. The hypervolume metric (or $\mathcal{S}$-metric) [32] is often used to evaluate the goodness of the Pareto set. The hypervolume indicator $\mathcal{H}(\mathcal{P})$ denotes the volume of the region in the objective space dominated by the Pareto set $\mathcal{P}$, bounded by a reference point $f^{max} + \varepsilon$, where $f^{max}$ denotes the anti-ideal point.

A better Pareto set has a higher corresponding hypervolume $\mathcal{H}(\mathcal{P})$. The contributing hypervolume $\mathcal{H}_{contr}(\mathbf{p}, \mathcal{P})$ of a Pareto set $\mathcal{P}$ relative to a point $\mathbf{p}$ (see Fig. 2) is defined as,

$$\mathcal{H}_{contr}(\mathbf{p}, \mathcal{P}) = \mathcal{H}(\mathcal{P} \cup \mathbf{p}) - \mathcal{H}(\mathcal{P}). \tag{6}$$

$\mathcal{H}_{\text{contr}}$ measures the contribution (or improvement) offered by the point $\mathbf{p}$ over the Pareto set $\mathcal{P}$ and can be used to define a scalar improvement function $I$ as,

$$I(\mathbf{p}, \mathcal{P}) = \begin{cases} \mathcal{H}_{\text{contr}}(\mathbf{p}, \mathcal{P}) & : \mathbf{p} \text{ is not dominated by } \mathcal{P} \\ 0 & : \text{otherwise.} \end{cases} \tag{7}$$

Let $y_j = f_j(\mathbf{x})$, $\hat{y}_j(\mathbf{x})$ be the prediction mean, and $s_j^2(\mathbf{x})$ be the prediction variance of a given surrogate model associated with the $j^{th}$ objective, then a Gaussian probability density function $\phi_j$ with mean $\hat{y}_j(\mathbf{x})$ and variance $s_j^2(\mathbf{x})$ can be defined as,

$$\phi_j[y_j] \triangleq \phi_j\left[y_j; \hat{y}_j(\mathbf{x}), s_j^2(\mathbf{x})\right]. \tag{8}$$

We use $\mathcal{H}_{\text{contr}}$ as the hypervolume contribution for $I$ in this work to compute the hypervolume-based probability of improvement (PoI) [8]. The hypervolume-based PoI can be written as the product of the improvement function $I(\hat{y}, \mathcal{P})$ and the multi-objective PoI $P[I]$,

$$P[I] = \int_{\mathbf{y} \in A} \prod_{j=1}^{m} \phi_j[y_j] dy_j, \tag{9}$$

$$P_{hv}[I] = I(\hat{\mathbf{y}}, \mathcal{P}) \cdot P[I], \tag{10}$$

where $\hat{\mathbf{y}} = (\hat{y}_1(\mathbf{x}), \ldots, \hat{y}_m(\mathbf{x}))$ is a vector containing the prediction of the models of each objective function for a point $\mathbf{x}$. The integration area $A$ of $P[I]$ corresponds to the non-dominated region. The reader is referred to Couckuyt et al. [8] for a detailed solution of Eq. 10.

### 3.2. Ensemble model construction and selection

The EMO algorithm couples a surrogate model with the hypervolume-based PoI criterion. The original formulation consisted of a fixed model type, i.e., Kriging. A modification is proposed in this paper which constructs an ensemble of multiple surrogate models (e.g., Kriging, SVR and RBF) in each iteration, and uses the most accurate one as determined using cross-validation to calculate the hypervolume-based PoI criterion.

This is helpful in situations where the practitioner does not know the most suitable surrogate model type beforehand, which can vary between applications. It minimizes the number of runs the practitioner has to go through to empirically find the most appropriate surrogate model, albeit at the expense of building multiple models per iteration.

The combined use of multiple surrogate models also allows for deficiencies of certain model types to be nullified, or lowered by other models over iterations. The overall goal of constructing multiple surrogate models is to boost the model accuracy.

### 3.3. Search strategy

Optimizing the hypervolume-based PoI can be complex as the optimization surface may be relatively flat with many local optima. Fortunately, as the criterion, and the underlying surrogate models can be evaluated cheaply, a hybrid Monte-Carlo based approach gives good results. Moreover, this approach allows multiple optima to be identified per iteration.

The sampling process typically consists of generating a large number of candidate samples in the design space, and using the hypervolume-based PoI criterion to rank the samples. The top-ranked candidate sample is fine-tuned by a local optimization method, evaluated and added to the training set. The model is then rebuilt using the updated training set.

In the original work [8], one sample is selected per iteration. Although, intuitively, selecting one point at a time maximizes the information gained in each iteration and thus is fairly optimal in minimizing the total number of samples, in many situations it is more desirable to pick multiple points per iteration (local optima) to speed up the optimization process. Since points can be evaluated in parallel, fewer surrogate models need to be built, thus saving time without compromising on performance.

Thereto, instead of selecting one candidate sample to fine-tune further, the $R$ top-ranked candidates are selected that are at least a given distance ($\epsilon$) apart from each other. Afterwards, each of the $R$ candidates is used as a starting point for a local optimization routine guided by the hypervolume-based PoI criterion. Optimized candidates that are separated by at least a distance of $\epsilon$ are retained and evaluated using the objective function(s).

## 4. Shape optimization of a cyclone separator

The typical geometrical layout of a gas cyclone separator used to separate particles from a gaseous stream is shown in Fig. 3, and corresponds to the Stairmand high-efficiency cyclone. The tangential inlet generates the swirling motion of the gas stream, which forces particles toward the outer wall where they spiral in the downward direction. Eventually the particles are collected in the dustbin (or flow out through a dipleg) located at the bottom of the conical section of the cyclone body. The cleaned gas leaves through the exit pipe at the top.

While the cyclone geometry is simple, the flow is an extremely complicated three dimensional swirling flow. The complexity of the gas solid flow pattern in cyclones has long been a matter of many experimental and theoretical studies. At present, Laser
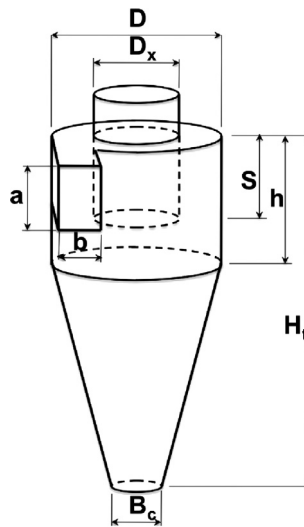
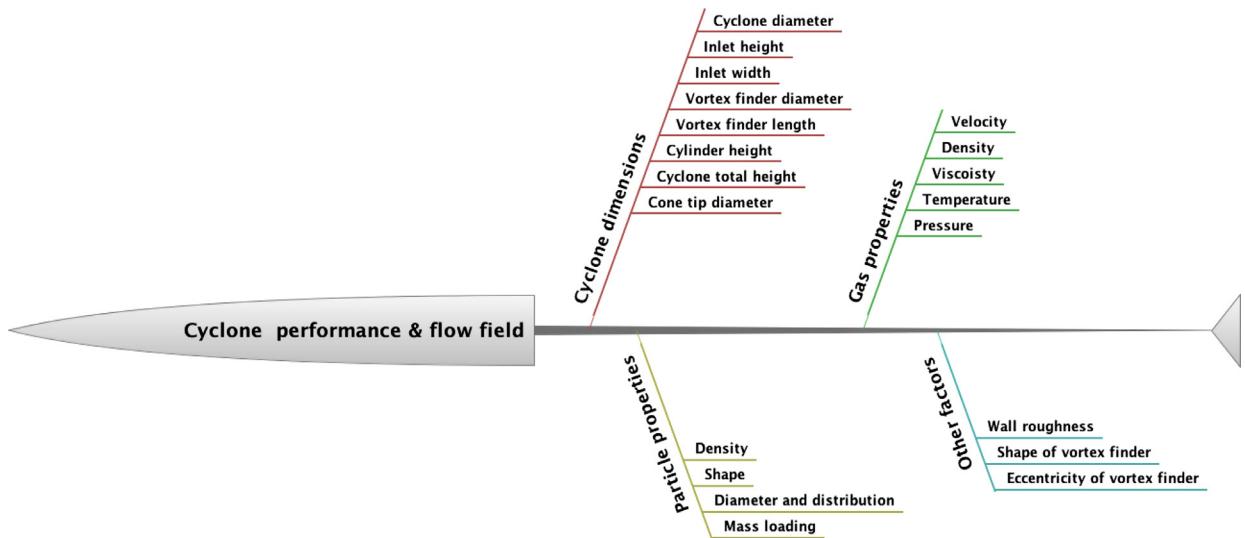**Fig. 3.** Schematic diagram of the gas cyclone separator.



**Fig. 4.** Cause and effect plot for a cyclone separator.

Doppler Anemometry (LDA) [33,34] and Particle Image Velocimetry (PIV) [35–37] are frequently employed to empirically study the flow structure in cyclones. As for the theoretical work, Computational Fluid Dynamics (CFD) simulation tools have proven to be useful for studying cyclonic flows [38–42].

The geometry of the cyclone affects the flow pattern and performance. The cyclone geometry is described by seven dimensions, namely, the cyclone inlet height $a$ and inlet width $b$, the gas outlet (vortex finder) diameter $D_x$ and length $S$, barrel height $h$, total height $H_t$ and cone-tip diameter $B_c$ [43] as shown in Fig. 3. All the parameters are given as the respective ratios of cyclone body diameter $D$.

The main factors influencing the cyclone performance and flow pattern are shown in Fig. 4, where the dominant factor is the cyclone geometry [43]. The two performance indicators widely used in low mass loading cyclones are the pressure drop and the cut-off diameter $x_{50}$ [43].

Several mathematical models are available in literature to estimate cyclone separator performance. Among these models, the Muschelknautz Method of modeling (MM), Ramachandran model and Iozia and Leith model are the most widely used models to predict the effect of geometry on the cyclone performance characteristics [43,44]. For a detailed discussion of these models, the interested reader is referred to Hoffmann and Stein [44] and Elsayed [43].

**Table 1**
Total number of objective function evaluations for each method.

| Method | # Evaluations | |
|---|---|---|
| | MM-Iozia | Ramachandran–Iozia |
| Kriging | 150 | 150 |
| RBF | 150 | 150 |
| SVR | 150 | 150 |
| Multi-surrogates | 150 | 150 |
| NSGA-II | 150 | 150 |
| NSGA-II | 10,000 | 10,000 |

*4.1. The pressure drop in a cyclone (Euler number)*

The dimensionless pressure drop (Euler number) is defined [44] as,

$$Eu = \frac{\Delta p}{\frac{1}{2}\rho V_{in}^2},$$ (11)

where $\Delta p$ is the pressure difference between the cyclone inlet and the gas exit, $\rho$ is the gas density and $V_{in}$ is the average inlet velocity [43].

The Euler number can be modeled using different models. Hoffmann and Stein [44] recommended the Muschelknautz Method of modeling (MM) [44–50]. According to the MM model, the pressure drop occurs mainly due to friction with the walls and irreversible losses throughout the vortex core [43].

As stated by Elsayed [43], the Ramachandran et al. [51] model is superior to Shepherd and Lapple [52], and Barth [53] models in comparison with experimental results. Consequently, this study considers only the Muschelknautz Method of modeling, and the Ramachandran model to estimate the Euler number.

*4.2. The cut-off diameter: the Iozia and Leith model (Stokes number)*

The cut-off diameter $x_{50}$ is the particle diameter that has a 50% collection efficiency [44]. The Stokes number [54] $Stk_{50}$ is the dimensionless cut-off diameter defined [43] as,

$$Stk_{50} = \rho_p x_{50}^2 V_{in}/(18\mu D).$$ (12)

It corresponds to the ratio between the particle relaxation time and the gas flow integral time scale [43], where $\rho_p$ is the particle density and $\mu$ is the gas viscosity. The Iozia and Leith model [55] is based on the equilibrium-orbit theory (Force balance) [44]. It exhibits good agreement with experimental data [43] and is used in this study to estimate the Stokes number.

## 5. Numerical settings

All experiments were performed using the SUMO Toolbox [19] for MATLAB®,[1] which is freely available for non-commercial use. The initial design is a Latin Hypercube [56] of 71 points. The hypervolume-based PoI sampling algorithm is used to select 5 new points in each iteration, until the simulation budget is exhausted. The distance threshold $\epsilon$ is set to 0.05. The simulation budget is 150 simulations for each simulator.

Each point is a 7-dimensional vector $\mathbf{x} = \{a, b, D_x, H_t, h, S, B_c\}$, and the MM-Iozia and Ramachandran–Iozia models are used to compute the value of the objectives, i.e., the Euler and Stokes numbers.

The EMO algorithm is applied using Kriging, RBF and SVR models independently. In addition, a novel strategy involving multi-surrogates described in Section 3.2 is employed which consists of the EMO algorithm using all three model types together. The most accurate model (determined using cross-validation) in each iteration is used with the hypervolume-PoI-based criterion to select new samples.

For the purpose of comparison, the well-known NSGA-II algorithm [14] is chosen for its robust performance and popularity. The population size is kept at 10 individuals, and a maximum of 15 generations are allowed. An additional run with a population size of 50 individuals evolving over 200 generations is also performed.

## 6. Results and discussion

The result of surrogate-based multi-objective optimization can be seen in Fig. 5. It can be seen that the Pareto set sufficiently covers the output space in all cases except for NSGA-II with 150 allowed function evaluations.

Table 1 lists the number of function evaluations for the experiments. Table 2 lists the hypervolume indicator of the Pareto sets obtained using each scheme. The values of the hypervolume indicator show that using multi-surrogates and SVR models with the EMO algorithm results in better Pareto-optimal solutions than when RBF models are used.

---

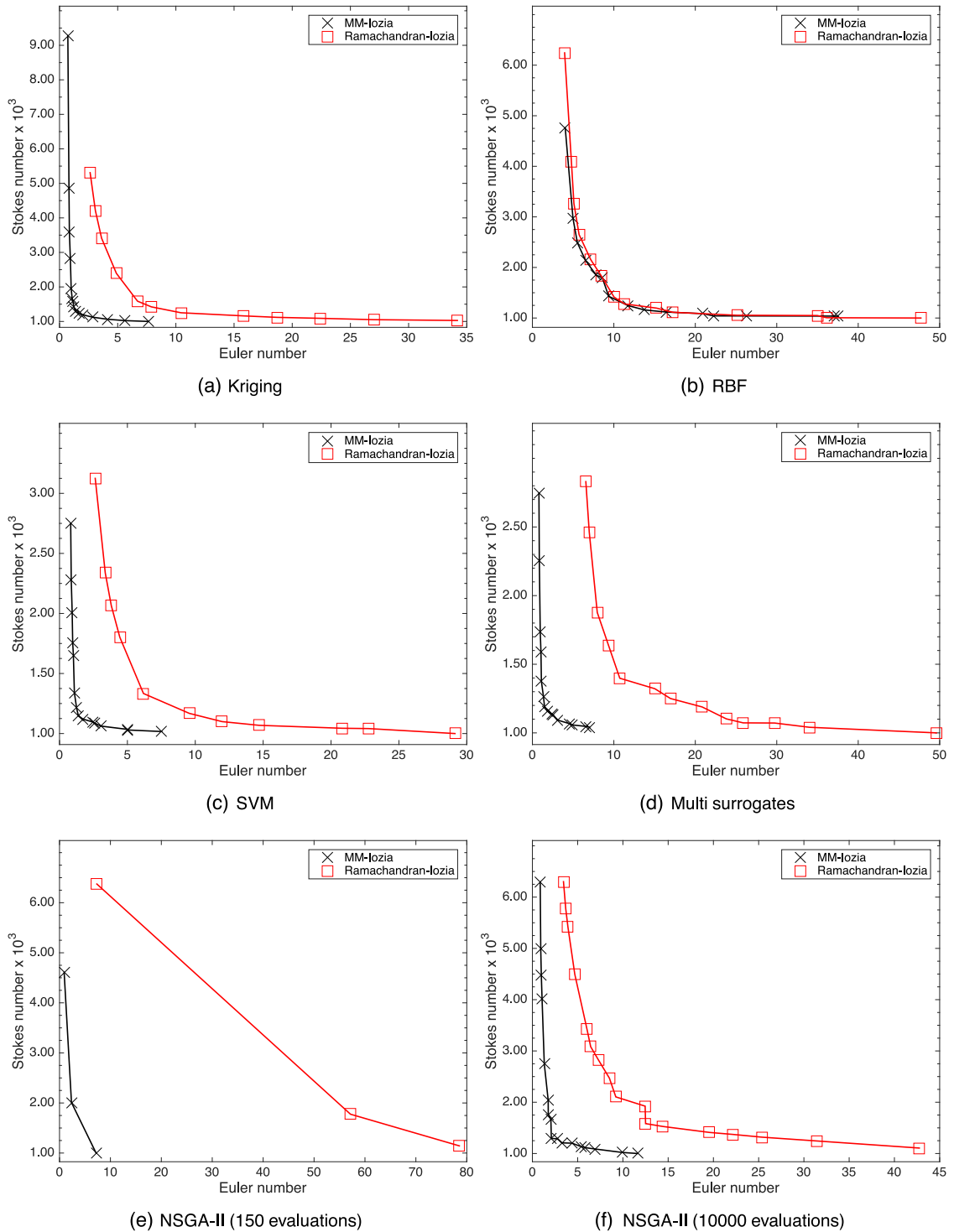[1] MATLAB, The MathWorks, Inc., Natick, Massachusetts, United States.

**Fig. 5.** The Pareto sets using the tested algorithms and the two tested simulators.

The final set of Pareto points corresponding to the 7 cyclone design dimensions obtained from all surrogates have similar Euler numbers. The shape of the cyclones at the knees of the Pareto sets are very close regardless of the simulator or surrogate model used. The extreme points have either a wider vortex finder (for minimum Euler number) or a narrow one to minimize the Stokes number. The shape of the Pareto fronts are similar for the same simulator regardless of the surrogate model type.

The model errors of trained surrogate models computed using cross-validation as measured using the Mean Squared Error (MSE) metric are also listed in Table 2. The results clearly show the benefits of using the multi-surrogates approach, as the

**Table 2**

Mean Squared Error (MSE), based on 5-fold cross-validation of trained surrogate models, and the hypervolume indicator for the resulting Pareto set for each method. The best results are highlighted in bold. The reference point used to estimate the hypervolume indicator is chosen to be the outermost point among all Pareto sets and has the value (3.8769, 1.8079) for the MM-Iozia simulator, and (4.3636, 1.8313) for the Ramachandran–Iozia simulator.

| Method | MSE | | | | Hypervolume indicator | |
|---|---|---|---|---|---|---|
| | MM-Iozia | | Ramachandran–Iozia | | MM-Iozia | Ramachandran–Iozia |
| | *Euler* | *Stokes* | *Euler* | *Stokes* | | |
| Kriging | 9.43e−05 | 1.07e−02 | 1.60e−04 | **7.89e−03** | 6.94 | 3.98 |
| RBF | 2.44e−03 | 1.26e−02 | 5.16e−02 | 1.03e−02 | 2.78 | 3.66 |
| SVR | 2.23e−04 | 1.28e−02 | 2.44e−04 | 1.90e−02 | 6.94 | **4.16** |
| Multi-surrogates | **5.75e−05** | **5.97e−03** | **1.09e−04** | 9.37e−03 | **6.96** | 3.81 |
| NSGA-II (150) | – | – | – | – | 5.32 | 4.24e−01 |
| NSGA-II (10,000) | – | – | – | – | 6.67 | 4.05 |

obtained models outperform all other model types. The exception is Kriging in the case of modeling Stokes number using the Ramachandran simulator. Kriging emerges as the single most accurate surrogate model type for the application across both cyclone models. However, it was observed that even though Kriging models are more accurate, SVR models resulted in comparable Pareto sets as reflected in Table 1 by the hypervolume indicator.

It is also interesting to analyze the performance gain of multi-surrogates over Kriging. Considering the case of the surrogate model obtained using multi-surrogates for Stokes number for the MM-Iozia simulator, the surrogate itself is a Kriging model. The improved accuracy can be attributed to the fact that even though RBF and SVR surrogates could not emerge as most accurate in the end, they did assist in performing better sampling in intermediate iterations where Kriging struggled. Consequently, the final surrogate model benefited in terms of accuracy. A similar behavior is also observed in both other cases where multi-surrogates approach is more accurate than Kriging alone. Also, since the sampling algorithm selects multiple new points per iteration, the optimization process is substantially quicker as compared to the original formulation of hypervolume-based PoI criterion.

Müller and Shoemaker [57] studied the influence of different surrogate model types, and sampling strategies on solution quality for global (single-objective) optimization of computationally expensive black-box functions. They consider RBF, Kriging and Spline models, and two- and three-member weighted ensembles thereof. It was found that ensembles typically outperformed single models, and the authors suggest using RBF in cases where the practitioner has no information about the objective function. The ensemble-based multi-surrogates approach performed well in this work too, as indicated by accurate models and the hypervolume indicator. In the multi-objective setting considered in this work, it was observed that Kriging models performed comparably or better than RBF models on the cyclone geometry optimization problem.

The Pareto set plots and the hypervolume indicator in Table 2 also show that the EMO algorithm has been able to provide solutions which are comparable to, or better than the solutions obtained using NSGA-II multi-objective evolutionary algorithm. The proposed approach offers the advantage of using substantially fewer number of function evaluations as compared to NSGA-II for providing comparable solutions (see Table 1). Considering the fact that the objective functions can be very expensive to evaluate (e.g., in case of CFD simulations), this advantage can translate into substantial time savings in the optimization process.

## 7. Conclusion and future work

The multi-objective shape optimization problem of a cyclone separator is solved using surrogate-based optimization, and the results are compared with those obtained using the NSGA-II algorithm. The surrogate model is trained with samples selected using the hypervolume-based probability of improvement criterion. A novel approach coupling an ensemble of multiple surrogate models (Kriging, RBF and SVR) with the hypervolume-based probability of improvement is described. The performance of different surrogate model types is validated on mathematical models of pressure loss in a cyclone. The insight gained from this analysis is helpful for the practitioner to select the best method for use with the expensive CFD simulations to save time. The results show that the proposed method solves the optimization problem using a very small simulation budget. The solutions obtained are comparable to those obtained using NSGA-II with only a fraction of objective function evaluations.

Future work includes optimizing the shape of a cyclone separator using CFD simulations in addition to mathematical models. As a single CFD simulation of a cyclone takes multiple weeks, analytical models will be used to reduce the computational burden. A combination of low and high fidelity simulators and analytical models used in tandem will be explored to minimize the time required for the optimization process.

# References

[1] P.K. Swamee, N. Aggarwal, K. Bhobhiya, Optimum design of cyclone separator, Am. Inst. Chem. Eng. (AIChE ) 55 (9) (2009) 2279–2283.
[2] G. Wang, S. Shan, Review of metamodeling techniques in support of engineering design optimization, J. Mech. Des. 129 (4) (2007) 370–380.
[3] D. Gorissen, I. Couckuyt, E. Laermans, T. Dhaene, Multiobjective global surrogate modeling, dealing with the 5-percent problem, Eng. Comput. 26 (2010) 81–98.
[4] J. Sacks, W.J. Welch, T.J. Mitchell, H.P. Wynn, Design and analysis of computer experiments, Stat. sci. 4 (4) (1989) 409–435.
[5] A. Sobester, S.J. Leary, A.J. Keane, On the design of optimization strategies based on global response surface approximation models, J. Glob. Optim. 33 (1) (2005) 31–59.
[6] H. Drucker, C.J.C. Burges, L. Kaufman, A.J. Smola, V. Vapnik, Support vector regression machines, in: Proceedings of the NIPS, 1996, pp. 155–161.
[7] S. Goasguen, S.M. Hammadi, S.M. El-Ghazaly, A global modeling approach using artificial neural network, in: Proceedings of IEEE MTT-S International Microwave Symposium Digest, 1, 1999, pp. 153–156, doi:10.1109/MWSYM.1999.779446.
[8] I. Couckuyt, D. Deschrijver, T. Dhaene, Fast calculation of multiobjective probability of improvement and expected improvement criteria for pareto optimization, J. Glob. Optim. 60 (3) (2014) 575–594.
[9] F. Viana, R. Haftka, Why not run the efficient global optimization algorithm with multiple surrogates? in: 51st AIAA/ASME/ASCE/AHS/ASC Structures, Structural Dynamics, and Materials Conference, 2010, pp. AIAA2010–3090.
[10] R. Badhurshah, A. Samad, Multiple surrogate based optimization of a bidirectional impulse turbine for wave energy conversion, Renew. Energy 74 (2015) 749–760.
[11] X.M. Chen, L. Zhang, X. He, C. Xiong, Z. Li, Surrogate-based optimization of expensive-to-evaluate objective for optimal highway toll charges in transportation network, Comput.-Aided Civ. Infrastruct. Eng. 29 (5) (2014) 359–381.
[12] M. Costas, J. Díaz, L. Romera, S. Hernández, A multi-objective surrogate-based optimization of the crashworthiness of a hybrid impact absorber, Int. J. Mech. Sci. 88 (2014) 46–54.
[13] S. Koziel, S. Ogurtsov, Numerically efficient approach to simulation-driven design of planar microstrip antenna arrays by means of surrogate-based optimization, in: Solving Computationally Expensive Engineering Problems, Springer, 2014, pp. 149–170.
[14] K. Deb, A. Pratap, S. Agarwal, T. Meyarivan, A fast and elitist multiobjective genetic algorithm: NSGA-II, IEEE Trans. Evol. Comput. 6 (2002) 182–197.
[15] N. Beume, B. Naujoks, M. Emmerich, SMS-EMOA: multiobjective selection based on dominated hypervolume, Eur. J. Oper. Res. 181 (3) (2007) 1653–1669.
[16] E. Zitzler, M. Laumanns, L. Thiele, SPEA2: Improving the Performance of the Strength Pareto Evolutionary Algorithm, Technical report, Swiss Federal Institute of Technology, 2001.
[17] A.I.J. Forrester, A.J. Keane, Recent advances in surrogate-based optimization, Prog. Aerosp. Sci. 45 (1–3) (2009) 50–79.
[18] I. Couckuyt, S. Koziel, T. Dhaene, Surrogate modeling of microwave structures using Kriging, co-Kriging, and space mapping, Int. J. Numer. Model.: electron. Netw. Devices Fields 26 (1) (2013) 64–73.
[19] D. Gorissen, I. Couckuyt, P. Demeester, T. Dhaene, K. Crombecq, A surrogate modeling and adaptive sampling toolbox for computer based design, J. Mach. Learn. Res. 11 (2010) 2051–2055.
[20] I. Couckuyt, T. Dhaene, P. Demeester, oodace toolbox: a flexible object-oriented Kriging implementation, J. Mach. Learn. Res. 15 (1) (2014) 3183–3186.
[21] S.N. Lophaven, H.B. Nielsen, J. Søndergaard, Aspects of the Matlab Toolbox DACE, Technical report, Informatics and Mathematical Modelling, Technical University of Denmark, DTU, Richard Petersens Plads, Building 321, DK-2800 Kgs. Lyngby, 2002.
[22] M. Stein, Interpolation of Spatial Data: Some Theory for Kriging, Springer-Verlag, 1999.
[23] D. Jones, C. Perttunen, B. Stuckman, Lipschitzian optimization without the lipschitz constant, Optim. Theory Appl. 79 (1) (1993) 157–181.
[24] T. Van Gestel, J.A. Suykens, B. Baesens, S. Viaene, J. Vanthienen, G. Dedene, B. De Moor, J. Vandewalle, Benchmarking least squares support vector machine classifiers, Mach. Learn. 54 (1) (2004) 5–32.
[25] J. Suykens, L. Lukas, P. Van Dooren, B. De Moor, J. Vandewalle, et al., Least squares support vector machine classifiers: a large scale algorithm, in: European Conference on Circuit Theory and Design, ECCTD, 99, 1999, pp. 839–842.
[26] J.A.K. Suykens, T.V. Gestel, J.D. Brabanter, B.D. Moor, J. Vandewalle, Least Squares Support Vector Machines, World Scientific, Singapore, 2002.
[27] T.V. Gestel, J. Suykens, G. Lanckriet, A. Lambrechts, B.D. Moor, J. Vandewalle, Bayesian framework for least squares support vector machine classifiers, gaussian processes and kernel fisher discriminant analysis, Neural Comput. 14 (5) (2002) 1115–1147.
[28] D. Jones, A taxonomy of global optimization methods based on response surfaces, J. Glob. Optim. 21 (4) (2001) 345–383.
[29] I. Couckuyt, F. Declercq, T. Dhaene, H. Rogier, L. Knockaert, Surrogate-based infill optimization applied to electromagnetic problems, Int. J. RF Microw. Comput.-Aided Eng. - Adv. Des. Optim. Microw.-RF Circuits Syst. 20 (5) (2010) 492–501.
[30] M. Emmerich, A. Deutz, J. Klinkenberg, Hypervolume-based expected improvement: monotonicity properties and exact computation, in: IEEE Congress on Evolutionary Computation (CEC), 2011.
[31] I. Couckuyt, D. Deschrijver, T. Dhaene, Fast calculation of multiobjective probability of improvement and expected improvement criteria for pareto optimization, J. Glob. Optim. (2013) 1–20.
[32] E. Zitzler, L. Thiele, M. Laumanns, C.M. Fonseca, V.G. Da Fonseca, Performance assessment of multiobjective optimizers: an analysis and review, Evol. Comput., IEEE Trans. 7 (2) (2003) 117–132.
[33] G. Solero, A. Coghe, Experimental fluid dynamic characterization of a cyclone chamber, Exp. Therm. Fluid Sci. 27 (2002) 87–96.
[34] L.Y. Hu, L.X. Zhou, J. Zhang, M.X. Shi, Studies on strongly swirling flows in the full space of a volute cyclone separator, AIChE J. 51 (3) (2005) 740–749.
[35] P.A. Yazdabadi, A.J. Griflths, N. Syred, Characterization of the PVC phenomena in the exhaust of a cyclone dust separator, Exp. Fluids 17 (1994) 84–95.
[36] T. O'Doherty, A.J. Griffiths, N. Syred, P.J. Bowen, W. Fick, Experimental analysis of rotating instabilities in swirling and cyclonic flows, Dev. Chem. Eng. Miner. Process. 7 (1999) 245–267.
[37] B. Zhang, S. Hui, Numerical simulation and PIV study of the turbulent flow in a cyclonic separator, in: International Conference on Power Engineering, Hangzhou, China, 2007.
[38] A.J. Hoekstra, J.J. Derksen, H.E.A. Van Den Akker, An experimental and numerical study of turbulent swirling flow in gas cyclones, Chem. Eng. Sci. 54 (1999) 2055–2065.
[39] W.D. Griffiths, F. Boysan, Computational fluid dynamics (CFD) and empirical modeling of the performance of a number of cyclone samplers, J. Aerosol Sci. 27 (2) (1996) 281–304.
[40] J. Gimbun, T.G. Chuah, T.S.Y. Choong, A. Fakhru'l-Razi, A CFD study on the prediction of cyclone collection efficiency, Int. J. Comput. Methods Eng. Sci. Mech. 6 (3) (2005) 161–168.
[41] J. Gimbun, T. Chuah, A. Fakhru'l-Razi, T.S.Y. Choong, The influence of temperature and inlet velocity on cyclone pressure drop: a CFD study, Chem. Eng. Process. 44 (1) (2005) 7–12.
[42] K. Elsayed, C. Lacor, Optimization of the cyclone separator geometry for minimum pressure drop using mathematical models and CFD simulations, Chem. Eng. Sci. 65 (22) (2010) 6048–6058.
[43] K. Elsayed, Analysis and Optimization of Cyclone Separators Geometry using RANS and LES Methodologies, Vrije Universiteit Brussel, 2011 Ph.D. thesis.
[44] A.C. Hoffmann, L.E. Stein, Gas Cyclones and Swirl Tubes: Principle, Design and Operation, second ed., Springer, 2008.
[45] E. Muschelknautz, W. Kambrock, Aerodynamische beiwerte des zyclon abscheiders aufgrund neuer und verbesserter messungen, Chem.-Ing.-Tech. 42 (5) (1970) 247–255.
[46] E. Muschelknautz, Die berechnung von zyklonabscheidern fur gas, Chem. Ing. Tech. 44 (1972) 63–71.
[47] E. Muschelknautz, M. Trefz, Design and calculation of higher and design and calculation of higher and highest loaded gas cyclones, in: Proceedings of Second World Congress on Particle Technology, Kyoto, Japan, 1990, pp. 52–71.

[48] M. Trefz, Die vershiedenen abscheidevorgange im hoher un hoch beladenen gaszyklon unter besonderer berucksichtigung der sekundarstromung, Forschritt-Berichte VDI; VDI-Verlag GmbH: Dusseldorf, Germany(1992) 295.
[49] M. Trefz, E. Muschelknautz, Extended cyclone theory for gas flows with high solids concentrations., Chem. Ing. Tech. 16 (1993) 153–160.
[50] C. Cortés, A. Gil, Modeling the gas and particle flow inside cyclone separators, Prog. Energy Combust. Sci. 33 (5) (2007) 409–452.
[51] G. Ramachandran, D. Leith, J. Dirgo, H. Feldman, Cyclone optimization based on a new empirical model for pressure drop, Aerosol Sci. Technol. 15 (1991) 135–148.
[52] C.B. Shepherd, C.E. Lapple, Flow pattern and pressure drop in cyclone dust collectors cyclone without intel vane, Ind. Eng. Chem. 32 (9) (1940) 1246–1248.
[53] W. Barth, Design and layout of the cyclone separator on the basis of new investigations, Brennstow-Wäerme-Kraft (BWK) 8 (4) (1956) 1–9.
[54] J.J. Derksen, S. Sundaresan, H.E.A. van den Akker, Simulation of mass-loading effects in gas–solid cyclone separators, Powder Technol. 163 (2006) 59–68.
[55] D.L. Iozia, D. Leith, Effect of cyclone dimensions on gas flow pattern and collection efficiency, Aerosol Sci. Technol. 10 (3) (1989) 491–500.
[56] F.A. Viana, G. Venter, V. Balabanov, An algorithm for fast optimal latin hypercube design of experiments, Int. J. Numer. Methods Eng. 82 (2) (2010) 135–156.
[57] J. Müller, C.A. Shoemaker, Influence of ensemble surrogate models and sampling strategy on the solution quality of algorithms for computationally expensive black-box global optimization problems, J. Glob. Optim. 60 (2) (2014) 123–144.